COMMUNICATION

Epitaxial Ferroelectric Heterostructures Fabricated by Selective Area Epitaxy of $SrRuO_3$ Using an MgO Mask

*J. Karthik, Anoop R. Damodaran, and Lane W. Martin**

We report the frequency-, cycling-, and temperature-dependent properties of symmetric $SrRuO_3/PbZr_{0.2}Ti_{0.8}O_3/SrRuO_3$ ferroelectric thin film capacitors with low leakage, improved fatigue properties, and excellent high-temperature stability. The critical advance that enables these high-performance structures is the development of a high-temperature, microfabrication-compatible hard mask that enables selective area epitaxy of $SrRuO_3$ top electrodes. This hard-mask is based on room-temperature growth and subsequent etching of the MgO using phosphoric acid. Here we apply these techniques to the development of high-temperature, epitaxial top contacts for ferroelectric thin films. We discuss the advantages of this hard-mask process and the global relevance of these contacts for advanced devices based on ferroelectrics and other functional oxide materials.

The combination of excellent thermal stability, mechanical toughness, radiation hardness, and desirable electrical properties (e.g., fast switching speeds, low power consumption, and high permittivity) have made ferroelectric materials candidates for non-volatile memories, advanced logic, infrared detectors, high density capacitors, electro-optic elements, and energy conversion systems.[1–8] In next generation nanoelectronics, for instance, the need for significant reductions in power consumption may be enabled by using ferroelectrics as replacements for high-κ dielectrics[2] and the selection of electrode materials possessing strong electronic correlations, including transition metal oxides, could lead to large and controllable deviations from geometric capacitance.[9,10] Furthermore, these materials must function well at temperatures above room temperature since integrated circuits operate at temperatures well above 100–150 °C (with higher transients).[11,12] As we look to integrate functional oxide materials, including ferroelectrics, into these devices it will be necessary to improve both contact materials and the processes by which we define them.

In the past decade, advances in sophisticated thin-film growth techniques have made ferroelectric (and multiferroic) materials strong candidates for modern technologies.[13,14] A number of scientific and technological challenges including fatigue, retention, and imprint have had to be addressed to enable such advances.[16] These effects have been shown to be dominated by defects (especially oxygen vacancies) and exacerbated by the choice of electrodes.[15–17] Certain electrodes are also known to reduce the permittivity and remnant polarization and increase the coercive field due to the appearance of a dead layer at the metal-ferroelectric interface.[18–23] While the intrinsic critical thickness for the occurrence of ferroelectricity is just a few unit cells (<5 nm)[19,24,25] the lack of perfect charge compensation in some metal electrodes often increases the practical usable thickness. A large number of experimental and theoretical studies have shown that oxide metals ($SrRuO_3$, $La_{0.5}Sr_{0.5}CoO_3$, SrO, etc.) perform significantly better than elemental metals as contacts due to their structural and chemical compatibility.[16,17,26,27] Such oxide metals improve fatigue and retention,[16] can help to minimize imprint,[17] help to prevent the formation of ferroelectric dead layers,[18–20] and result in large permittivity and remnant polarization even in ultrathin ferroelectric layers.[20]

At the same time, the use of ferroelectrics at high temperature has also been severely restricted by the lack of high-temperature compatible electrodes and contact-based experimental measurements of ferroelectric thin film properties at temperatures above room temperature are, therefore, rarely reported. Increased leakage, diminished chemical stability, and poor adhesion of electrodes at elevated temperatures has made this particularly difficult. Furthermore, electrode asymmetry has also been shown to affect temperature dependent properties adversely.[28] As a result, researchers have focused on non-contact techniques (e.g., second harmonic generation[29,30] and X-ray diffraction (XRD)[31]) to probe temperature dependent properties of thin films, but quantitative measures of ferroelectric properties are hard to obtain with these techniques. Thus, the practical utility of ferroelectric materials is, in many cases, limited by the electrodes used to contact them and the intrinsic properties of ferroelectrics can be completely obscured by the extrinsic effects originating from the metal-ferroelectric interface.[20,22] Therefore the fabrication of capacitor structures with nearly ideal metal-ferroelectric interfaces is crucial for optimizing the performance of ferroelectrics, extending their temperature of operation, and in obtaining fundamental insights into the intrinsic properties.

In this work we focus on 150 nm $PbZr_{0.2}Ti_{0.8}O_3$/20 nm $SrRuO_3/DyScO_3$ (DSO) (110) heterostructures grown via pulsed-laser deposition.[32] X-ray diffraction studies of the resulting heterostructures (**Figure 1**A) reveal single-phase, high-quality thin films. Detailed off-axis and reciprocal space mapping studies (RSMs) reveal that these films are fully epitaxial and coherently strained to the underlying substrate. A RSM about the 103-psuedocubic diffraction condition reveals that both the $PbZr_{0.2}Ti_{0.8}O_3$ and $SrRuO_3$ possess the same in-plane lattice parameter as the $DyScO_3$ substrate (Figure 1B). The resulting films are also found to be smooth and using atomic force microscopy we have observed root-mean-square surface roughness of ~0.5 nm (Figure 1C).

J. Karthik, A. R. Damodaran, Prof L. W. Martin
Department of Materials Science and Engineering and Materials Research Laboratory
University of Illinois
Urbana-Champaign, Urbana, IL 61801, USA
E-mail: lwmartin@illinois.edu

DOI: 10.1002/adma.201104697

© 2012 WILEY-VCH Verlag GmbH & Co. KGaA, Weinheim

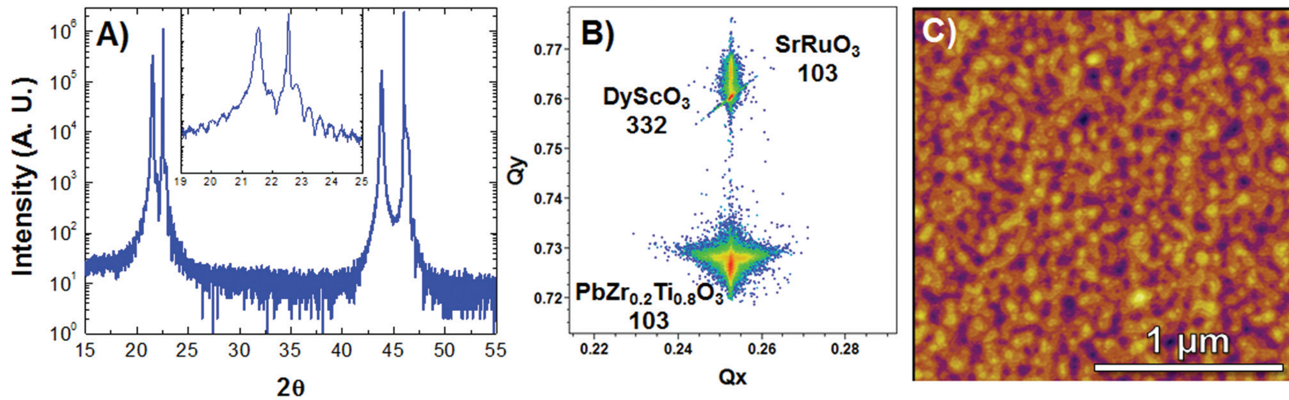

Figure 1. A) θ–2θ X-ray diffraction pattern about the 002-diffraction peak for the $SrRuO_3/PbZr_{0.2}Ti_{0.8}O_3/SrRuO_3$ thin film heterostructure. B) Reciprocal space map about the pseudocubic 103-diffraction conditions. C) Atomic force microscopy image of a typical $PbZr_{0.2}Ti_{0.8}O_3/SrRuO_3/DyScO_3$ (110) thin film.

To create capacitor device structures, we have developed a novel new process that differs considerably from traditional techniques. In prior work, following the growth of an oxide metal bottom electrode and ferroelectric layer, elemental or oxide metal top electrodes are typically deposited at room temperature through a standard photoresist mask, unwanted material is removed via lift-off, and, in some cases, the capacitor structure is post-annealed. Even in capacitors with the same top- and bottom-electrode material, the resulting contacts are not identical. In some cases, a tri-layer stack has been grown in situ and top contacts have been defined by ion-milling.[20] Ion-milling, however, can induce mechanical damage and overmilling is difficult to avoid due to the lack of chemical selectivity. High temperature metal oxide deposition through a shadow mask has also been explored,[33] but shadow masks suffer from large feature sizes and poor registry. Thus, existing methods for defining top electrodes are not adequate for fabricating epitaxial metal-ferroelectric-metal structures for advanced applications. A lithography based technique would be ideal, but defining features with photoresist prevents further epitaxial growth due to the poor high-temperature stability of photoresists. In this work, we use a novel MgO hard-mask process to fabricate epitaxial all-oxide heterostructures and utilize this process to make nearly ideal, symmetric capacitor structures with excellent ferroelectric properties and high-temperature stability.

The new process is described in **Figure 2**A. Following the growth of the $PbZr_{0.2}Ti_{0.8}O_3/SrRuO_3$ heterostructures, we spin coat photoresist and expose/develop the inverse of the desired final device pattern. Then a 200 nm layer of amorphous MgO is deposited at room temperature by e-beam evaporation. The unwanted photoresist and MgO are lifted off in acetone. The remaining MgO layer serves as the hard mask for the subsequent deposition of the top $SrRuO_3$ electrode in the desired pattern. Before proceeding to the high-temperature deposition of the top oxide metal, we perform an oxygen-plasma cleaning step to remove any remaining photoresist residue on the surface of the ferroelectric layer. The MgO hard mask/$PbZr_{0.2}Ti_{0.8}O_3$/$SrRuO_3$ heterostructure is then pumped to a base pressure of ~1×10^{-6} Torr, the chamber is flooded to a pressure of 760 Torr of oxygen, and the sample is heated to a deposition temperature of 500–600 °C. Before deposition, the chamber is quickly evacuated to a growth pressure of 100 mTorr and (in this case) 80 nm of $SrRuO_3$ is deposited. Following growth, films are cooled to room temperature at an oxygen pressure of 760 Torr.

After growth, the $SrRuO_3$ is lifted off by etching the MgO in a 15% solution of phosphoric acid. The phosphoric acid etches the MgO at a rapid rate (~7.5 nm/sec.) (Figure 2B), but does not appear to impact the surface or nature of the other oxides (etching rates for $PbZr_{0.2}Ti_{0.8}O_3$ and $SrRuO_3$ are estimated to be <0.1 nm/sec.). Using this technique and

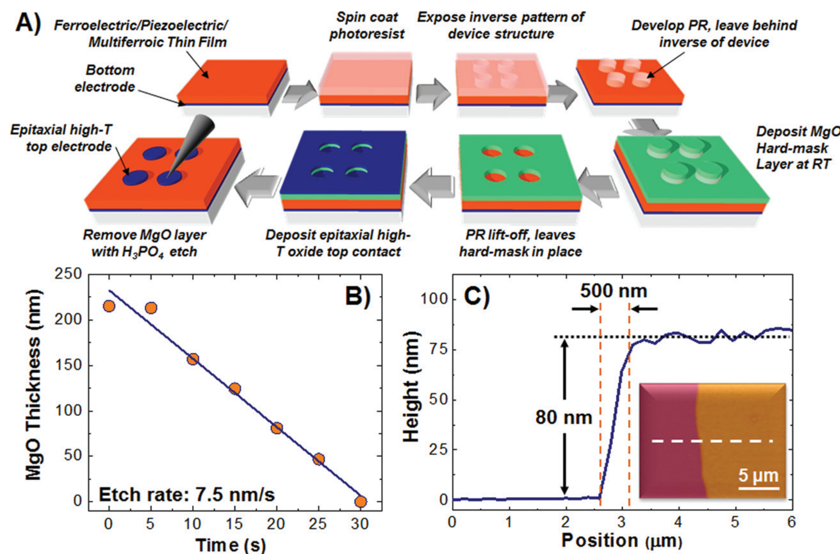

Figure 2. A) Schematic of the process to fabricate epitaxial top electrodes using an MgO hard mask. B) Etching rate of MgO in a 15% solution of phosphoric acid. C) A topography scan obtained with atomic force microscope across the edge of a circular capacitor (inset) showing the edge definition and thickness of $SrRuO_3$ deposited as the top electrode using an MgO mask.

© 2012 WILEY-VCH Verlag GmbH & Co. KGaA, Weinheim

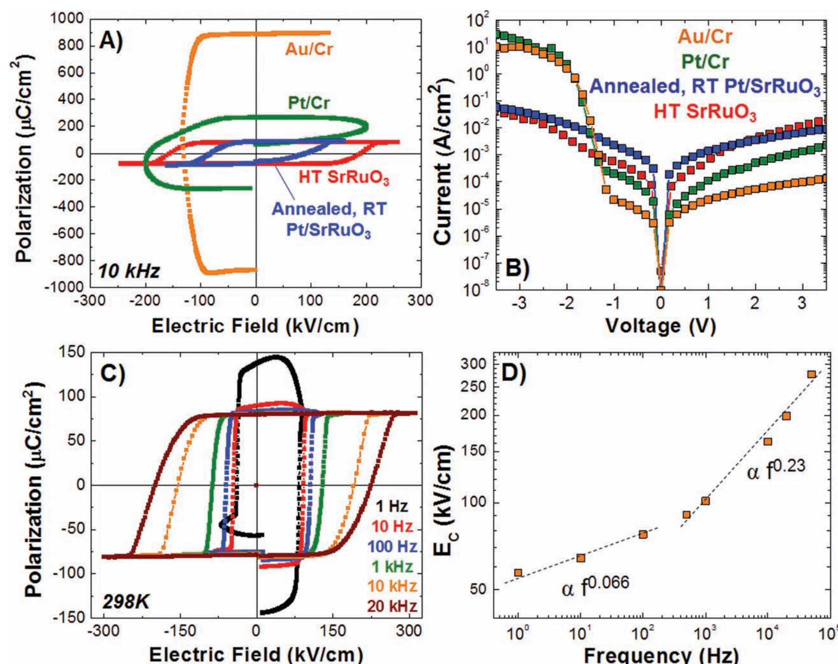

Figure 3. A) Ferroelectric hysteresis loops obtained at 300 K and 10 kHz for four different top contacts. B) Current-voltage data for the various top electrodes at 300 K. C) Room-temperature ferroelectric hysteresis loops for high-temperature $SrRuO_3$ top electrode capacitors. D) Coercive field (E_c) as a function of frequency reveals good agreement with the Ishibashi model of growth controlled domain switching.

traditional optical lithography, features down to 8 μm in lateral dimension have been fabricated (Supporting Information, Figure S1). The process also results in well defined, abrupt edges (Figure 1C). Thus far we have been limited by the temperature of decomposition of the ferroelectric layer and not by that of the hard-mask. We have, however, investigated the stability and etchability of the MgO after higher temperature treatments and have found that even after annealing the MgO features at 1200 °C for 1 hour (Supporting Information, Figure S2) we observe similar etch rates for the MgO. Work to date suggests that the MgO process described here is compatible with any modern nanolithography process and thus we anticipate this process could be extended to smaller feature sizes with ease. The ultimate minimum feature sizes will be dependent not on the MgO process, but on the minimum feature size achievable by the given patterning technique. The MgO process described herein can be thought to be complementary to the recent use of anodic aluminum oxide (AAO) masks used to fabricate nanofeatures of ferroelectrics at high temperature[34] and subsequent use of AAO and electron-beam lithography/lift-off techniques to define nanoscale top-contacts for ferroelectrics.[35] The current approach provides addition high-temperature stability for the fabrication of epitaxial oxide contacts and since it does not rely on the AAO process allows for the generation of arbitrary shapes and feature sizes.

We have investigated the ferroelectric properties of the capacitor structures using a wide range of techniques. To demonstrate the importance of contacts in controlling the ferroelectric properties, we have created four different ferroelectric capacitors for comparison using the same $PbZr_{0.2}Ti_{0.8}O_3$/$SrRuO_3$/$DyScO_3$ (110) heterostructures. We have investigated the following top contacts: 1) 100 nm Au/5 nm Cr, 2) 100 nm Pt/5 nm Cr, 3) room-temperature deposited 100 nm Pt/80 nm $SrRuO_3$ followed by annealing at 600 °C for 30 min in oxygen, and 4) high-temperature deposited 80 nm $SrRuO_3$ electrodes using the MgO hard-mask process described above. Ferroelectric polarization electric field hysteresis loops measured on these samples (**Figure 3**A) reveal that while elemental metal contacts exhibit hysteresis loops dominated by leakage, hysteresis loops improve significantly with the annealed Pt/$SrRuO_3$ contacts. The capacitors fabricated with epitaxial $SrRuO_3$ electrodes, however, exhibit the best performance with symmetric, square loops.

The effect of the various electrodes on the current-voltage and leakage characteristics of the capacitors was also studied (Figure 3B). The metal-ferroelectric-metal structure can be understood as back-to-back Schottky diodes[28,33] and at any applied voltage the Schottky diode that is under reverse-bias will dominate the leakage characteristics. Here the bottom electrode was fixed at ground and the drive voltage was applied to the top electrode. Thus, for positive and negative voltages, the bottom and top interfaces dominate the leakage characteristics, respectively. Since the bottom electrode is essentially identical for all samples, the leakage current at positive voltages is expected to be similar. For negative voltages, however, the leakage is dominated by the top electrode interface with transition metals such as Cr (with a low work function and high electronegativity) exhibiting a poor rectifying contact[33] that gives rise to asymmetric leakage characteristics and lossy hysteresis loops. Noble metals such as Au and Pt should give rise to better electrical performance, but exhibit poor adhesion without an adhesion layer of Cr, Ti, etc. The $SrRuO_3$ electrodes, however, dramatically reduce the leakage and imprint due to the higher work function (4.5–5 eV)[36] and the chemical compatibility of the interface.

Focusing now on the samples with the high-temperature, epitaxial $SrRuO_3$ top electrodes, we have investigated the room-temperature ferroelectric response of these films between 1 and 2 × 10^4 Hz (Figure 3C). Generally, low frequency hysteresis loops are difficult to measure due to the dominance of leakage currents and one usually resorts to high frequencies (> 1 kHz) to measure reliable loops. This has made the frequency-dependent study of ferroelectric properties difficult, especially for undoped $PbZr_{0.2}Ti_{0.8}O_3$ films. The combination of high-quality $PbZr_{0.2}Ti_{0.8}O_3$ films and symmetric epitaxial electrodes results in robust ferroelectric response with square ferroelectric hysteresis loops, large remnant polarization (P_r ~ 79 μC/cm^2), negligible polarization offsets and loop closure even at measurement frequencies of 10 Hz. Even at 1 Hz, the films reveal evidence of ferroelectric switching (although somewhat convoluted by the DC leakage). These measurement frequencies are one to two orders-of-magnitude lower than measurements

© 2012 WILEY-VCH Verlag GmbH & Co. KGaA, Weinheim

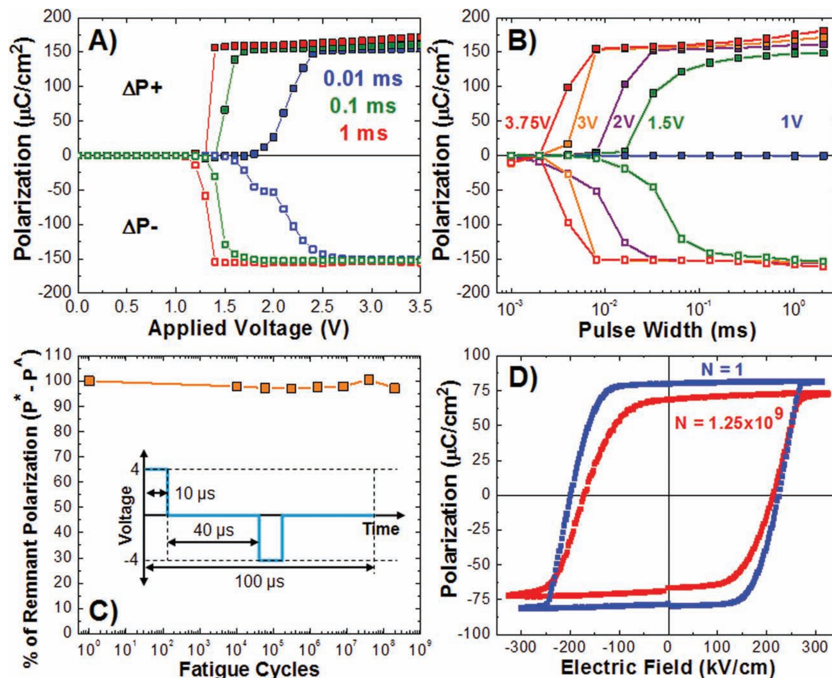

Figure 4. PUND measurement as a function of A) voltage for various pulse widths and B) pulse width for various pulse voltages. C) Fatigue data showing the loss of remnant polarization (P_r) with repeated cycling. D) Ferroelectric hysteresis loops of the capacitor shown in C) in the as grown state (N = 1) and after N = 1.25 × 10^9 cycles; data taken 5 minutes after the fatigue measurement.

typically done using traditional contacts for similar films. From these measurements, we can extract the frequency dependence of coercive voltage (Figure 3D). We have determined the coercive voltage as $E_c = (|E_{c+}| + |E_{c-}|)/2$ where E_{c+} and E_{c-} are the positive and negative coercive fields from the hysteresis loop. We see that coercive voltage can be described by a power law of the form $E_c \sim f^{\beta}$ as predicted from domain wall motion limited models of ferroelectric switching.[37] This is consistent with earlier work[1,38,39] which demonstrated that domain wall growth rather than nucleation should play an important role in ferroelectric switching in epitaxial films. We observe two scaling regimes with different β and a crossover frequency of ~300 Hz. The presence of two scaling regimes is likely due to the presence of two frequency dependent regimes of domain wall switching.[38,39] At low frequencies thermally activated creep of domain walls controls switching, but at high frequencies, in the absence of sufficient time for the creep to completely switch the polarization, the viscous flow of the domain wall dominates.

We have also probed the switching and fatigue properties of our samples via pulsed measurements. Polarization fatigue is the process by which switchable ferroelectric polarization is reduced by repetitive electrical cycling and is among the most serious device failure mechanisms in ferroelectric films. Traditionally, it has been suggested that ferroelectric capacitors with elemental metal electrodes suffer significant fatigue and that simply replacing the elemental metal with an oxide metal improves the fatigue performance.[1,15,16,26,27,40–44] Since oxygen vacancy accumulation at the metal-ferroelectric interface is a major cause of fatigue, the oxide metals perform better since they serve to compensate for the oxygen vacancies. We begin with PUND switching measurements with bipolar pulses which were completed as a function of applied voltage (**Figure 4**A) and pulse width (Figure 4B). For these capacitors, we observe symmetric and complete switching for positive and negative biases occurring at +/− 1.4 V (93.3 kV/cm), 1.6 V (106.6 kV/cm), and 2.5 V (166.6 kV/cm), for 1 ms, 0.1 ms, and 0.01 ms pulses, respectively. Likewise, we observe the onset of switching only for voltages in excess of 1 V and critical pulse durations ranging from 0.002–0.016 ms for voltages ranging from 3.75 to 1.5 V. This shows that complete switching can be obtained in these films at 10 μs with voltage pulses as small as 2.5 V. This information was used to complete a study of the fatigue properties of these capacitors using a bipolar pulse train (described in the inset of Figure 4C) with a 4 V pulse at a frequency of 10 kHz with a 20% duty cycle. The samples are found to possess essentially no fatigue even after 10^8–10^9 cycles. Furthermore, after 1.25 × 10^9 cycles the measured remnant polarization was 69 μC/cm^2 just five minutes after completion of the fatigue and returned to essentially the same pre-fatigue levels after a few days (Figure 4D).

Temperature dependent ferroelectric characterization was also performed between 296–430 K (**Figure 5**); roughly 100 K higher than measurements reported previously. The temperature stable top electrodes enabled square hysteresis loops to be obtained up to 430 K (Figure 5A). Elemental metals or room-temperature deposited $SrRuO_3$ are known to give lossy hysteresis loops or to completely fail at temperatures >373 K.[28] This makes the temperature dependence of polarization (or pyroelectric coefficient) and coercive field very difficult to obtain. Often, one resorts to phase sensitive techniques to

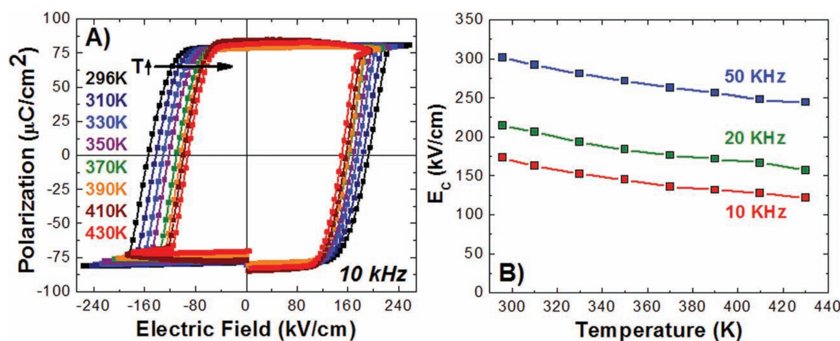

Figure 5. A) Temperature-dependent hysteresis loops of a symmetric, high-temperature capacitor structure. B) Coercive field (E_c) as a function of temperature at various frequencies.

© 2012 WILEY-VCH Verlag GmbH & Co. KGaA, Weinheim

measure the temperature dependence of polarization to offset the problems of DC leakage and thermally stimulated currents.[45] From our temperature-dependent hysteresis loops, we can estimate a pyroelectric coefficient for $PbZr_{0.2}Ti_{0.8}O_3$ as 0.033 $\mu C/cm^2K$ (assuming a constant pyroelectric coefficient across the temperature range 300–400 K) (Supporting Information, Figure S3). Further, the temperature dependence of coercive field (Figure 5B) shows that the coercive field decreases roughly linearly with temperature in this regime with a slope of 0.6 kV/cm-K. The frequency- and temperature-dependent characterization give useful insights into the intrinsic behavior of $PbZr_{0.2}Ti_{0.8}O_3$ films and show that ferroelectric film performance can be greatly improved with the choice of electrodes.

In conclusion, we have developed an MgO-based hard-mask process to fabricate epitaxial heterostructures of complex oxide materials and utilized the process to synthesize ferroelectric $PbZr_{0.2}Ti_{0.8}O_3$ capacitor structures with epitaxial $SrRuO_3$ electrodes. The capacitors thus fabricated reveal excellent ferroelectric properties and enhanced high-temperature stability. Apart from improving the performance of ferroelectrics, the ability to fabricate such patterned epitaxial ferroelectric structures should provide fundamental insights to the properties of these materials without the debilitating effects arising from poor contacts. We anticipate that this process can be widely applicable in other exciting oxide systems, such as colossal magnetoresistive oxides, high-temperature superconductors, and in the study of novel properties of oxide interfaces across a wide range of length scales and temperatures.

Supporting Information

Supporting Information is available from the Wiley Online Library or from the author.

Acknowledgements

J.K. and L.W.M. acknowledge support from the Office of Naval Research under grant number N00014-10-10525. A.R.D. and L.W.M. acknowledge support from the Army Research Office under grant number W911NF-10-1-0482. Experiments were carried out in part in the Frederick Seitz Materials Research Laboratory Central Facilities, which are partially supported by the U.S. Department of Energy under grants DE-FG02-07ER46453 and DE-FG02-07ER46471.

Received: December 8, 2011
Revised: January 22, 2012
Published online: February 22, 2012

[1] J. F. Scott, *Ferroelectric Memories* (Springer, Berlin, **2000**).
[2] S. Salahuddin, S. Datta, *Nano. Lett.* **2009**, *8*, 405.
[3] D. G. Schlom, S. Guha, S. Datta, *MRS Bull.* **2008**, *33*, 1017.
[4] M. Dawber, K. M. Rabe, J. F. Scott, *Rev. Mod. Phys.* **2005**, *77*, 1083.
[5] J. F. Scott, *Science* **2007**, *315*, 954.
[6] J. F. Scott, C. A. Araujo, H. B. Meadows, L. D. McMillan, A. Shawabkeh, *J. Appl. Phys.* **1989**, *66*, 1444.
[7] T. Choi, S. Lee, Y. J. Choi, V. Kiryukhin, S.-W. Cheong, *Science* **2009**, *324*, 63.
[8] S. Y. Yang, J. Seidel, S. J. Byrnes, P. Shafer, C.-H. Yang, M. D. Rossell, P. Yu, Y.-H. Chu, J. F. Scott, J. W. Ager, III, L. W. Martin, R. Ramesh, *Nat. Nanotechnol.* **2010**, *5*, 143.
[9] T. Kopp, J. Mannhart, *J. Appl. Phys.* **2009**, *106*, 064504.
[10] J. Mannhart, D. G. Schlom, *Science* **2010**, *327*, 1607.
[11] T.-Y. Wang, C.-P. Chen, *IEEE Trans. Comp. Aided Design Integ. Circ. Systems* **2002**, *21*, 1434.
[12] W. Huang, E. Humenay, K. Skadron, M. R. Stan, *Proc. of the 2005 Inter. Symp. Low Power Electronics and Design*, Aug. 08-10, **2005**, San Diego, CA (doi: 10.1145/1077603.1077662).
[13] D. G. Schlom, L.-Q. Chen, C.-B. Eom, K. M. Rabe, S. K. Streiffer, J.-M. Triscone, *Ann. Rev. Mater. Res.* **2007**, *37*, 589.
[14] L. W. Martin, Y.-H. Chu, R. Ramesh, *Mater. Sci. Eng. R* **2010**, *68*, 89.
[15] M. Dawber, J. F. Scott, *Appl. Phys. Lett.* **2000**, *76*, 1060.
[16] A. K. Tagantsev, I. Stolichnov, E. L. Colla, N. Setter, *J. Appl. Phys.* **2001**, *90*, 1387.
[17] T. Morimoto, O. Hidaka, K. Yamakawa, O. Arisumi, H. Kanaya, T. Iwamoto, Y. Kumura, I. Kunishima, S. Tanaka, *Jpn. J. Appl. Phys.* **2000**, *39*, 2110.
[18] V. Nagarajan, S. Prasertchoung, T. Zhao, H. Zheng, J. Ouyang, R. Ramesh, W. Tian, X. Q. Pan, D. M. Kim, C.-B. Eom, H. Kohlstedt, R. Waser, *Appl. Phys. Lett.* **2004**, *84*, 5225.
[19] G. Gerra, A. K. Tagantsev, N. Setter, K. Parlinski, *Phys. Rev. Lett.* **2006**, *96*, 107603.
[20] Y. S. Kim, J. Y. Jo, D. J. Kim, Y. J. Chang, J. H. Lee, T. W. Noh, T. K. Song, J.-G. Yoon, J.-S. Chung, S. I. Baik, Y.-W. Kim, C. U. Chung, *Appl. Phys. Lett.* **2006**, *88*, 072909.
[21] M. Stengel, D. Vanderbilt, N. A. Spaldin, *Nat. Mater.* **2009**, *8*, 392.
[22] A. K. Tagantsev, M. Landivar, E. Colla, N. Setter, *J. Appl. Phys.* **1995**, *78*, 2623.
[23] N. A. Pertsev, J. Rodriguez Contreras, V. G. Kukhar, B. Hermanns, H. Kohlstedt, R. Waser, *Appl. Phys. Lett.* **2003**, *83*, 3356.
[24] J. Junquera, P. Ghosez, *Nature* **2003**, *422*, 506.
[25] D. D. Fong, G. B. Stephenson, S. K. Streiffer, J. A. Eastman, O. Auciello, P. H. Fuoss, C. Thompson, *Science* **2004**, *304*, 1650.
[26] C. B. Eom, R. B. Van Dover, Julia M. Phillips, D. J. Werder, J. H. Marshall, C. H. Chen, R. J. Cava, R. M. Fleming, D. K. Fork, *Appl. Phys. Lett.* **1993**, *63*, 2570.
[27] B. Nagaraj, S. Aggarwal, R. Ramesh, *J. Appl. Phys.* **2001**, *90*, 375.
[28] L. Pintilie, I. Vrejoiu, D. Hesse, G. LeRhun, M. Alexe, *Phys. Rev. B* **2007**, *75*, 104103.
[29] M. Fiebig, V. V. Pavlov, R. V. Pisarev, *J. Opt. Soc. Am. B* **2005**, *22*, 96.
[30] K. J. Choi, M. Biegalski, Y. L. Li, A. Sharan, J. Schubert, R. Uecker, P. Reiche, Y. B. Chen, X. Q. Pan, V. Gopalan, L. Q. Chen, D. G. Schlom, C. B. Eom, *Science* **2004**, *306*, 1005.
[31] C. H. Yang, J. Seidel, S. Y. Kim, P. B. Rossen, P. Yu, M. Gajek, Y. H. Chu, L. W. Martin, M. B. Holcomb, Q. He, P. Maksymovych, N. Balke, S. V. Kalinin, A. P. Baddorf, S. R. Basu, M. L. Scullin, R. Ramesh, *Nat. Mater.* **2009**, *8*, 485.
[32] The films were grown at 630 °C with the $SrRuO_3$ bottom electrode and $PbZr_{0.2}Ti_{0.8}O_3$ layers being grown in 100 and 200 mTorr of oxygen, laser repetition rates of 12 and 3 Hz, and laser fluences of 1.75 and 2 J/cm^2, respectively. Following growth, films are cooled to room temperature at an oxygen pressure of 760 Torr.
[33] L. Pintilie, I. Vrejoiu, D. Hesse, M. Alexe, *J. Appl. Phys.* **2008**, *104*, 114101.
[34] W. Lee, H. Han, A. Lotnyk, M. A. Schubert, S. Senz, M. Alexe, D. Hesse, S. Baik, U. Gösele, *Nat. Nanotechnol.* **2008**, *3*, 402.
[35] Y. Kim, H. Han, B. J. Rodriguez, I. Vrejoiu, W. Lee, S. Baik, D. Hesse, M. Alexe, *J. Appl. Phys.* **2010**, *108*, 042005.
[36] A. J. Hartmann, M. Neilson, R. N. Lamb, K. Watanabe, J. F. Scott, *Appl. Phys. A.* **2000**, *70*, 239.
[37] Y. Ishibashi, H. Orihara, *Integrated Ferroelectrics* **1995**, *9*, 57.

© 2012 WILEY-VCH Verlag GmbH & Co. KGaA, Weinheim

[38] S. M. Yang, J. Y. Jo, T. H. Kim, J.-G. Yoon, T. K. Song, H. N. Lee, Z. Marton, S. Park, Y. Jo, T. W. Noh, *Phys. Rev. B* **2010**, *82*, 174125.
[39] Y. W. So, D. J. Kim, T. W. Noh, J.-G. Yoon, T. K. Song, *Appl. Phys. Lett.* **2005**, *86*, 092905.
[40] Y. Masuda, T. Nozaka, *Jpn. J. Appl. Phys.* **2003**, *42*, 5941.
[41] S. Aggarwal, I. G. Jenkins, B. Nagaraj, C. J. Kerr, C. Canedy, R. Ramesh, G. Velasquez, L. Boyer, J. T. Evans Jr., *Appl. Phys. Lett.* **1999**, *75*, 1787.
[42] I. Stolichnov, A. Tagantsev, N. Setter, J. S. Cross, M. Tsukuda, *Appl. Phys. Lett.* **1999**, *74*, 3552.
[43] W. Wu, K. H. Wong, C. L. Choy, Y. H. Zhang, *Appl. Phys. Lett.* **2000**, *77*, 3441.
[44] M. Kobune, O. Matsuura, T. Matsuzaki, A. Mineshige, S. Fujii, H. Fujisawa, M. Shimizu, H. Niu, *Jpn. J. Appl. Phys.* **2000**, *39*, 5451.
[45] E. J. Sharp, Lynn E. Garn, *J. Appl. Phys.* **1982**, *53*, 8980.

© 2012 WILEY-VCH Verlag GmbH & Co. KGaA, Weinheim